



UNIVERSITÀ  
DEGLI STUDI  
FIRENZE

# FLORE

## Repository istituzionale dell'Università degli Studi di Firenze

### An Interferometric MIMO Radar for Bridge Monitoring

Questa è la Versione finale referata (Post print/Accepted manuscript) della seguente pubblicazione:

*Original Citation:*

An Interferometric MIMO Radar for Bridge Monitoring / Massimiliano Pieraccini; Lapo Miccinesi. - In: IEEE GEOSCIENCE AND REMOTE SENSING LETTERS. - ISSN 1545-598X. - ELETTRONICO. - (2019), pp. 1-5. [10.1109/LGRS.2019.2900405]

*Availability:*

This version is available at: 2158/1151012 since: 2020-01-08T11:33:10Z

*Published version:*

DOI: 10.1109/LGRS.2019.2900405

*Terms of use:*

Open Access

La pubblicazione è resa disponibile sotto le norme e i termini della licenza di deposito, secondo quanto stabilito dalla Policy per l'accesso aperto dell'Università degli Studi di Firenze (<https://www.sba.unifi.it/upload/policy-oa-2016-1.pdf>)

*Publisher copyright claim:*

Conformità alle politiche dell'editore / Compliance to publisher's policies

Questa versione della pubblicazione è conforme a quanto richiesto dalle politiche dell'editore in materia di copyright.

This version of the publication conforms to the publisher's copyright policies.

(Article begins on next page)

# An Interferometric MIMO Radar for Bridge Monitoring

Massimiliano Pieraccini<sup>ID</sup>, *Member, IEEE*, and Lapo Miccinesi<sup>ID</sup>, *Student Member, IEEE*

**Abstract**—The authors propose an interferometric multiple-input multiple-output radar specifically designed for monitoring/testing bridges. It makes use of compressive sensing and synthetic aperture radar techniques for providing coherent images of its field of view. The radar prototype has been tested in controlled environment and in operative conditions during the static test of a pedestrian bridge.

**Index Terms**—Compressive sensing (CS), ground-based synthetic aperture radar (SAR), multiple-input multiple output (MIMO), radar.

## I. INTRODUCTION

SINCE the early 2000s ground-based interferometric radar systems have been proposed for monitoring/testing bridges [1]–[3]. Currently, this equipment is routinely used in civil engineering practice [4]–[10] and also in emergency situations. As an example, after the tragic collapse of the “Morandi” highway bridge at Genova (Italy) [11], the fire fighters installed two interferometric radar for monitoring the remains of the bridge still standing.

These interferometric radars exploit the movement of the radar head along a mechanical guide for providing 2-D images of the structure under test; therefore, their acquisition speed is intrinsically limited by the mechanical system. Currently, the fastest radar in the market is able to acquire in 4 s [12]. A great advance could be an interferometric radar without moving parts: it could be potentially much faster and robust.

In 2013, Tarchi *et al.* [13] designed an interferometric multiple-input multiple-output (MIMO) radar. The disposition of antennas was carefully studied for reducing the grating lobes that typically affect this kind of radar. Hu *et al.* [14] and Michellini *et al.* [15] proposed radar systems based on a similar approach.

Unlike the radar mentioned above, the interferometric MIMO proposed in this letter, the pattern of antennas is random and the spatial sampling is recovered by compressive sensing (CS) techniques. The advantage of this approach is that the radar has better angular resolution than a conventional dense MIMO with the same number of antennas. Indeed,

the  $4 \times 4$  implementation described in this letter reconstructs 40 “virtual antennas” by 16 physical centers of phase. It means an improvement of angular resolution of a factor of 2.5 with respect to a dense  $4 \times 4$  MIMO.

## II. WORKING PRINCIPLE OF THE RADAR

The radar operates using a step-frequency continuous wave transceiver that transmits  $N_f$  frequencies from  $f_1$  to  $f_2$  at step  $\Delta f$ . A set of microwave cables and switches connects the transmitting channel of the transceiver with  $N_{TX}$  transmitting antennas and the receiving channel with  $N_{RX}$  receiving antennas.

With reference to Fig. 1, two parallel mechanical guides have  $N_p$  notches at step  $\lambda/2$  in correspondence of which it is possible to fix the antennas.  $N_{TX} < N_p$  antennas are positioned along one of the guide.  $N_{RX} < N_p$  antennas are positioned along the other one. By switching on and off all the antennas, the number of possible independent acquisitions is  $M = N_{TX} \times N_{RX}$ .

Generally speaking, when the TX antenna in the  $i$ th position and the RX antenna in the  $j$ th position are both switched on (and all the others switched off), it is equivalent (in far field) to transmit and receive with one single “virtual” antenna along the median axis in the position  $(i + j)/2$ . Therefore, for each combination of the TX and RX antennas, a specific pattern along the median axis is defined. This pattern can be seen as a random sampling of the electromagnetic field backscattered by the targets in the field of view of the radar.

The Nyquist theorem would require that spatial step has to be smaller than a quarter of wavelength ( $\lambda/4$ ) for omnidirectional antennas (this constraint is a bit more relaxed for directional antennas, but it is not essential in the discussion that follows). Nevertheless, in recent years, the advanced processing techniques named CS have been developed [16], [17]. These techniques assert one can recover certain signals from far fewer samples or measurements than traditional methods use. Its basic idea relies on the “sparsity” of the signals of interest (the radar signals typically have this property [18]), and the incoherence of the sensing modality. The later property is obtained through the random sampling. Following the approach reported in [19], CS techniques have been applied independently for each transmitted frequency for obtaining the matrix  $E_{k,l}$ , with  $k$ -index ranging from 1 to  $N_f$  and  $l$ -index ranging from 1 to  $N$ , number of virtual antennas  $\lambda/4$  spaced.

The next step is to focus the matrix  $E_{k,l}$  using a back-propagation algorithm that takes into account the phase history

Manuscript received November 19, 2018; revised January 8, 2019 and February 16, 2019; accepted February 17, 2019. (Corresponding author: Massimiliano Pieraccini.)

The authors are with the Department of Information Engineering, University of Florence, 50139 Florence, Italy (e-mail: massimiliano.pieraccini@unifi.it; lapo.miccinesi@unifi.it).

Color versions of one or more of the figures in this letter are available online at <http://ieeexplore.ieee.org>.

Digital Object Identifier 10.1109/LGRS.2019.2900405

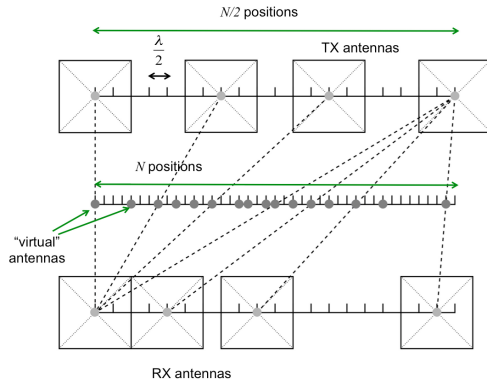


Fig. 1. Sampling along the linear mechanical guide of a GBSAR.

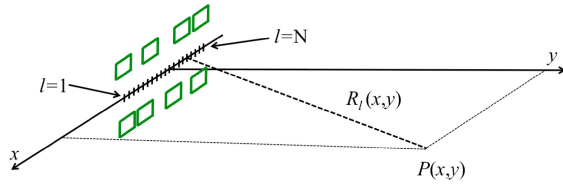


Fig. 2. Focusing geometry.

of each single contribution (relative to a specific  $l$ th position and a specific  $k$ th frequency).

With reference to Fig. 2, the image value  $I(x, y)$  in a generic image point  $P(x, y)$  can be calculated as

$$I(x, y) = \sum_{k=1}^{N_f} \sum_{i=1}^N E_{k,i} e^{\sqrt{-1} \frac{4\pi}{c} f_k R_i(x, y)} \quad (1)$$

where  $c$  is the speed of light. Equation (1) can be calculated through FFT and interpolation as shown, for example, in [20].

Since  $I(x, y)$  is a complex number, it provides the phase information too. This can be exploited for generating differential interferograms. Displacement maps can be obtained from differential interferograms using the well-known relationship [1]

$$\Delta r(x, y) = \frac{\lambda}{4\pi} \Delta \varphi(x, y) \quad (2)$$

where  $\Delta r(x, y)$  is the displacement in the point  $P(x, y)$ ,  $\Delta \varphi(x, y)$  is the differential phase in the point  $P(x, y)$ , and  $\lambda$  is the wavelength at the center frequency.

### III. RADAR PROTOTYPE

Fig. 3 shows the block scheme of the radar prototype. The vector network analyzer (HP8720D) operates as transceiver.

The switching system consists of eight single-pole double-through (SPDT) mod. MSP2T-18-12+ and ten high phase stability ( $\pm 0.5^\circ$ ) microwave cables (SUCOFLEX 126). Another couple of SPDT provides a calibration path (with a  $-40$  dB power attenuator). A relay board controls the switching system. The calibration path and all the paths between VNA and each antennas are of the same electromagnetic length in order to avoid any further calibration procedure. Fig. 4 shows a photograph of the radar head.

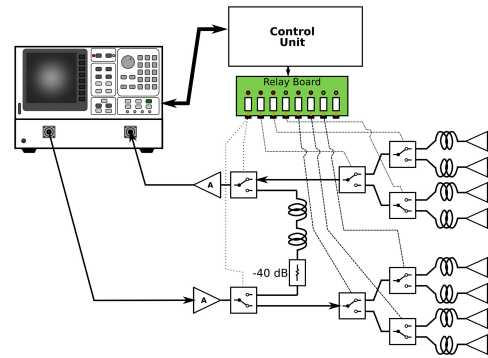


Fig. 3. Block scheme of the radar prototype.

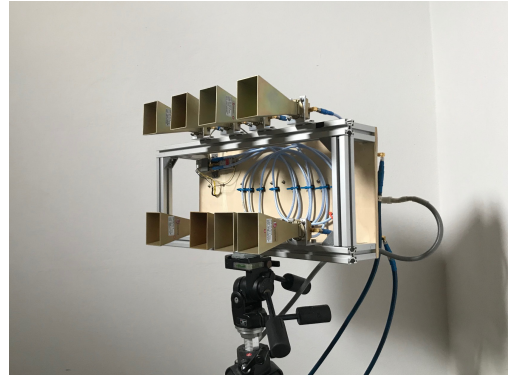


Fig. 4. Photograph of the radar head.

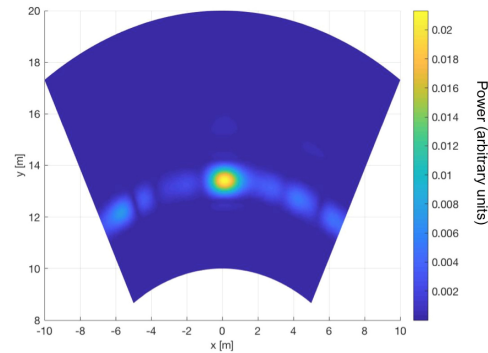


Fig. 5. Radar image of a CR in front of the radar.

### IV. PRELIMINARY EXPERIMENTAL TESTS

The MIMO radar has been preliminary tested in a controlled experimental test site. In an open garden, a single corner reflector (CR) of 0.4 m side length was positioned at 13.4 m in front of the radar. The measurement parameters were:  $f_1 = 9.84$  GHz,  $f_2 = 10.16$  GHz, and  $N_f = 801$ . Fig. 5 shows the obtained radar image.

The red line in Fig. 6 is the power plot in azimuth at the distance of the CR. The blue line is the power plot obtained by simulating one point scatterer in front of the radar. The agreement between the two plots is very good.

As the CS performance depends critically on the view angle, we repeated the measurement moving the CR 2.80 m on the

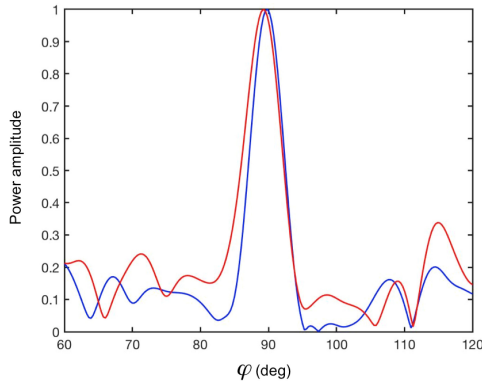


Fig. 6. Experimental (red line) and simulated (blue line) power plots in azimuth of a CR in front of the radar.

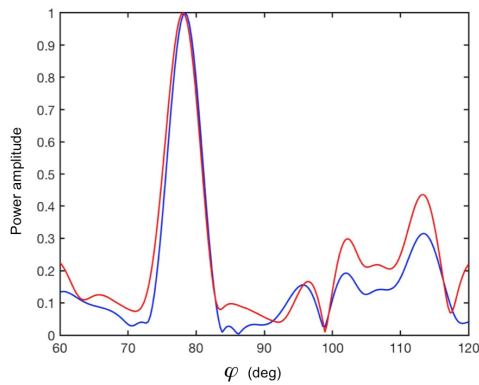


Fig. 7. Experimental (red line) and simulated (blue line) power plots in azimuth of a CR on the left side.

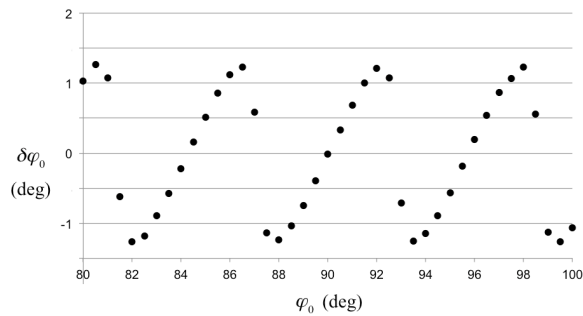


Fig. 8. Error in the azimuth angle estimation by varying the azimuth angle.

right. Fig. 7 shows the measured and simulated power plots. Note that the angle  $\varphi$  is between the  $x$ -axis and the view direction, so  $90^\circ$  is in front of the radar and  $\varphi < 90^\circ$  is on the right side.

It is interesting to note that the simulated and measured plots have a small misalignment that cannot be easily corrected. Indeed, it is an effect of the nonlinearity of the CS recovery. In order to verify this statement, we have simulated the response of a single target at 13.4 m distance with  $\varphi_0$  azimuth angle varying from  $80^\circ$  to  $100^\circ$  at step of  $0.5^\circ$ . The error  $\delta\varphi_0$  in the azimuth recovered using the CS has the nonlinear behavior shown in Fig. 8.

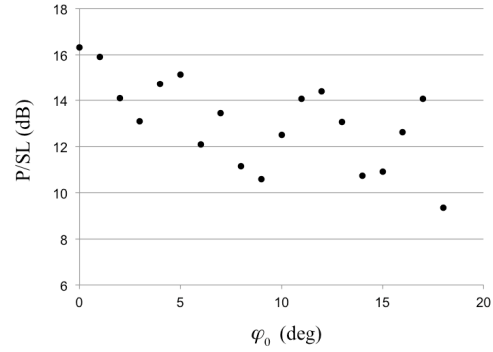


Fig. 9. P/SL for a single target at 13.4 m distance at the azimuth angle between  $0^\circ$  and  $18^\circ$  at  $1^\circ$  step.

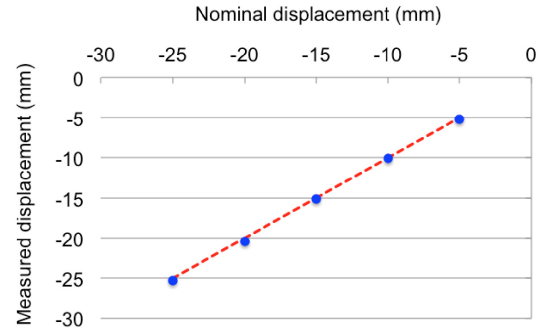


Fig. 10. CR displacements detected by radar.

A critical point of any radar is the amplitude of the sidelobes. For a CS radar, this value could be rather erratic. With the aim of evaluate it, we simulated the response of a single target at 13.4 m distance at  $\varphi_0$  azimuth. The plot in Fig. 9 shows the peak to sidelobe ratio (P/SL) in function of  $\varphi_0$ .

We have considered only the sidelobes inside the antenna lobe ( $\pm 20^\circ$ ). It results that if the target is inside a view cone  $\pm 15^\circ$  the P/SL is always larger than 10 dB.

In order to test the capability of MIMO to detect displacement by interferometry, we put the CR on a micropositioner with 0.1 mm nominal accuracy. We moved the CR forward the radar at step of 5 mm. Fig. 10 shows the obtained results. The agreement with nominal values is better than 0.2 mm.

## V. TEST OF A PEDESTRIAN BRIDGE

The radar prototype has been in-field operated for monitoring a pedestrian bridge at Poggibonsi, Italy. In 2007, the same bridge was tested with an interferometric radar. The experimental results were published in [21] and [22].

The MIMO radar was installed close to one of the two pillars of bridge, as shown in Fig. 11. The bridge spans 45.7 m.

The measurement parameters were: initial frequency  $f_1 = 9.84$  GHz, final frequency  $f_2 = 10.16$  GHz, number of frequencies  $N_f = 801$ . Therefore, the range resolution was 0.47 m and the unambiguous range 375 m. The antenna aperture in the horizontal plan was about  $\pm 20^\circ$ . The transmitted power was 12 dBm. The radar completed a single acquisition in 31.4 s. Fig. 12 shows a picture of the radar installation.

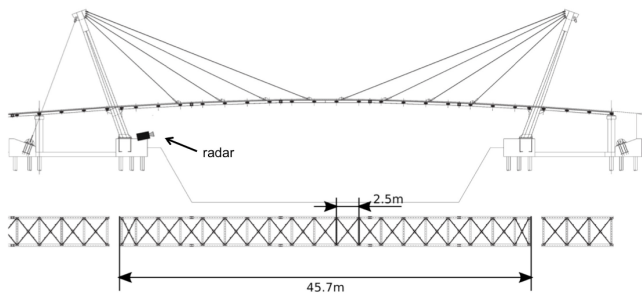


Fig. 11. Pedestrian bridge of Poggibonsi, Italy.



Fig. 12. Photograph of the radar installation.

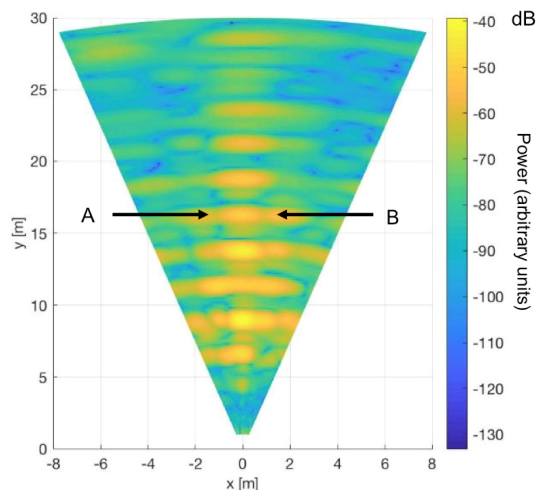


Fig. 13. Radar image of the lower deck of the bridge.

Fig. 13 shows the obtained power image of the lower deck. The first nine transversal beams are well imaged. The shape of the deck is recognizable. Unfortunately, due to the low transmitted power (12 dBm), the transversal beams are hardly visible in the portion of the deck farther than 24 m.

The bridge was loaded with a small car (900 kg). It slowly went to the median point and came back. In order to evidence the effects of an asymmetric load the car was driven as on the left as it was possible (the bridge is wide 2.8 m, while the car was 1.6 m wide) as shown in Fig. 14.



Fig. 14. Test of the bridge using a small car as load.

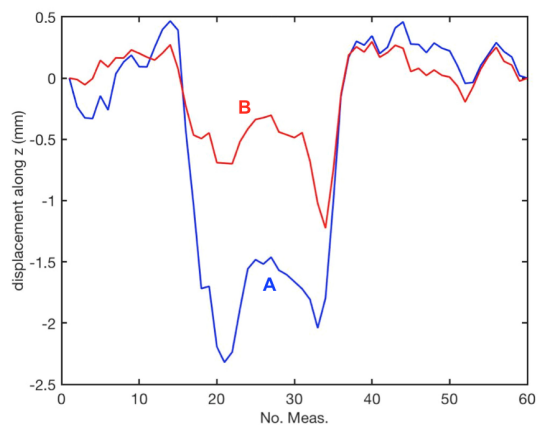


Fig. 15. Plots of the displacements of points A and B.

Fig. 15 shows the detected displacements (projected in vertical direction) of the points A (on the left side of the deck) and B (on the right side of the deck) during the loading and downloading operations. In the  $x$ -axis, there is the number of acquisition. The radar acquired an image each 31.4 s. Both the points are at 16.18 m range, very close to the center of the span. The car was slowly driven until to the center of span and it stayed there for about 12 min. As expected the point on the left had a larger displacement (about 2.0 mm). The difference of displacement between left and right sides is about 1 mm.

We note at the beginning of measurement session a slight uplift of the deck. In effect, as the pillars were about 10 m inside the riverbed (see Fig. 11), when the car entered the bridge from one side the center of the span rose. Furthermore, the car passed the center and came back, so the plot in time shows two peaks (at 21st and 33rd measurements).

## VI. CONCLUSION

A MIMO has been designed and successfully tested as geotechnical equipment for testing bridges. The radar has been tested in controlled environment and the experimental results have been compared with the simulations. An in-field test has been performed during a static test of bridge. The radar has been able to resolve different displacements of points at the same range.

The sampling time of the radar prototype is about 30 s, but this relatively long time is due to the specific VNA that

TABLE I

SPECIFICATIONS/PERFORMANCE OF THE PROPOSED MIMO RADAR

Owner/manufacturer/customer	University of Florence, Italy
Name/acronym	CS-MIMO
Goal	Research
Radar type	VNA based
Band	X
Polarization	VV
Acquisition time for one image	31.4 s
Scan	Electronic scan
Range resolution	0.47 m
Azimuth resolution	50 mrad
Nominal precision	0.1 mm

operated as transceiver. It was an old model (HP8720D) not designed for fast operation. In effect, as this radar does not have mechanical moving parts, it could acquire much faster than the current GB synthetic aperture radar (SAR) based on the movement of a radar head along a mechanical linear guide. A fast interferometric radar can have single-tone integration time of  $10 \mu\text{s}$  [2] with the number of frequency  $N_f = 500$ . It means an acquisition time of 20 ms using four antennas. A radar with 2-D imaging capability (provided by the MIMO architecture) operating at this acquisition speed (50 Hz) opens exciting perspectives in the field of health monitoring and testing of large structure.

For the sake of simplicity, the radar is provided with eight antennas. This configuration can give high side clutter with targets at more than  $10^\circ$ – $20^\circ$  with respect to direction of view. Nevertheless, a MIMO based on the same working principle could be used for monitoring targets with larger angular extension (like building or slopes) by increasing the number of antenna. In our opinion a MIMO with  $8 \times 8$  antennas could cover the majority of applications.

Finally, in order to directly compare the proposed radar with existing radar systems, Table I reports the main specifications/performance as suggested in [5].

We would like to notice that the radar proposed in this letter has performances comparable to many existing GB-SAR, but it does not have mechanical moving parts and uses only eight antennas.

## REFERENCES

- [1] M. Pieraccini *et al.*, "Structural static testing by interferometric synthetic radar," *NDT E Int.*, vol. 33, no. 8, pp. 565–570, 2000.
- [2] M. Pieraccini, M. Fratini, F. Parrini, and C. Atzeni, "Dynamic monitoring of bridges using a high-speed coherent radar," *IEEE Trans. Geosci. Remote Sens.*, vol. 44, no. 11, pp. 3284–3288, Nov. 2006.
- [3] M. Pieraccini, F. Parrini, M. Fratini, C. Atzeni, P. Spinelli, and M. Micheloni, "Static and dynamic testing of bridges through microwave interferometry," *NDT E Int.*, vol. 40, no. 3, pp. 208–214, 2007.
- [4] M. Pieraccini, "Monitoring of civil infrastructures by interferometric radar: A review," *Sci. World J.*, vol. 2013, Aug. 2013, Art. no. 786961. doi: 10.1155/2013/786961.
- [5] O. Monserrat, M. Crosetto, and G. Luzi, "A review of ground-based SAR interferometry for deformation measurement," *ISPRS J. Photogram. Remote Sens.*, vol. 93, pp. 40–48, Jul. 2014.
- [6] T. Owerko, L. Ortyl, R. Kocierz, P. Kuras, and M. Salamak, "Investigation of displacements of road bridges under test loads using radar interferometry—Case study," in *Proc. 6th Int. Conf. Bridge Maintenance, Saf., Manage., Resilience Sustainability*, Stresa, Italy, Jul. 2012, pp. 181–188.
- [7] T. A. Stabile, A. Perrone, M. R. Gallipoli, R. Ditommaso, and F. C. Ponzio, "Dynamic survey of the Musmeci bridge by joint application of ground-based microwave radar interferometry and ambient noise standard spectral ratio techniques," *IEEE Geosci. Remote Sens. Lett.*, vol. 10, no. 4, pp. 870–874, Jul. 2013.
- [8] L. Mayer, B. S. Yanev, L. D. Olson, and A. W. Smyth, "Monitoring of Manhattan bridge for vertical and torsional performance with GPS and interferometric radar systems," in *Proc. 89th Annu. Meeting Transp. Res. Board*, Washington, DC, USA, Jan. 2010, pp. 1–7.
- [9] C. Gentile, "Deflection measurement on vibrating stay cables by non-contact microwave interferometer," *NDT E Int.*, vol. 43, no. 3, pp. 231–240, 2010.
- [10] D. Beben, "Application of the interferometric radar for dynamic tests of corrugated steel plate (CSP) culvert," *NDT E Int.*, vol. 44, no. 5, pp. 405–412, 2011.
- [11] *Italy Bridge: Dozen Feared Dead in Genoa as Motorway Collapses*. Accessed: Mar. 6, 2019. [Online]. Available: <https://www.bbc.com/news/world-europe-45183624>
- [12] S. Roedelsperger, A. Coccia, D. Vicente, C. Trampuz, and A. Meta, "The novel FastGBSAR sensor: Deformation monitoring for dike failure prediction," in *Proc. Asia-Pacific Conf. Synthetic Aperture Radar (APSAR)*, Sep. 2013, pp. 420–423.
- [13] D. Tarchi, F. Oliveri, and P. F. Sammartino, "MIMO radar and ground-based SAR imaging systems: Equivalent approaches for remote sensing," *IEEE Trans. Geosci. Remote Sens.*, vol. 51, no. 1, pp. 425–435, Jan. 2013.
- [14] C. Hu, J. Wang, W. Tian, T. Zeng, and R. Wang, "Design and imaging of ground-based multiple-input multiple-output synthetic aperture radar (MIMO SAR) with non-collinear arrays," *Sensors*, vol. 17, no. 3, p. 598, Mar. 2017.
- [15] A. Michelini, F. Coppi, A. Bicci, and G. Alli, "SPARX, a MIMO array for ground-based radar interferometry," *Sensors*, vol. 19, no. 2, p. 252, Feb. 2019.
- [16] E. J. Candes and M. B. Wakin, "An introduction to compressive sampling," *IEEE Signal Process. Mag.*, vol. 25, no. 2, pp. 21–30, Mar. 2008.
- [17] R. G. Baraniuk, "Compressive sensing [lecture notes]," *IEEE Signal Process. Mag.*, vol. 24, no. 4, pp. 118–121, Jul. 2007.
- [18] M. A. Hadi, S. Alshebeili, K. Jamil, and F. E. A. El-Samie, "Compressive sensing applied to radar systems: An overview," *Signal, Image Video Process.*, vol. 9, no. 1, pp. 25–39, 2015.
- [19] L. Miccinesi, N. Rojhani, and M. Pieraccini, "Compressive sensing for no-contact 3D ground penetrating radar," in *Proc. 41st Int. Conf. Telecommun. Signal Process.*, Athens, Greece, Jul. 2018, pp. 1–5.
- [20] M. Pieraccini and L. Miccinesi, "ArcSAR: Theory, simulations, and experimental verification," *IEEE Trans. Microw. Theory Techn.*, vol. 65, no. 1, pp. 293–301, Jan. 2007.
- [21] M. Pieraccini, M. Fratini, F. Parrini, C. Atzeni, and G. Bartoli, "Interferometric radar vs. Accelerometer for dynamic monitoring of large structures: An experimental comparison," *NDT E Int.*, vol. 41, no. 4, pp. 258–264, 2008.
- [22] D. Dei, M. Pieraccini, M. Fratini, C. Atzeni, and G. Bartoli, "Detection of vertical bending and torsional movements of a bridge using a coherent radar," *NDT E Int.*, vol. 42, pp. 741–747, Dec. 2009.